

# Quadrupolar Interactions

Pascal P. Man

Université Pierre et Marie Curie, Paris, France

1	Introduction	1
2	Quadrupolar Hamiltonian in a Uniform Space	2
3	Spherical Tensor Representation for the Quadrupolar Hamiltonian	2
4	Quadrupolar Interaction as a Perturbation of Zeeman Interaction	3
5	Energy Levels and the Spectrum of a Single Crystal	3
6	Powder Spectrum	6
7	Appendix	8
8	Related Articles	9
9	References	10

## 1 INTRODUCTION

Nuclei are characterized by an atomic number  $Z$ , a mass number  $A$ , and a nuclear spin  $I$ . The value of  $I$  depends on those of  $A$  and  $Z$  (Table 1). Nuclei with spin  $I > \frac{1}{2}$  are multiple energy level systems and are called quadrupolar nuclei. They represent more than 70% of those in the Periodic Table. However, they are not as frequently investigated in NMR as other elements, because of their quadrupole moments  $Q$ , which interact with the electric field gradient (EFG) generated by their surroundings. This coupling, called the quadrupolar interaction and denoted by  $\mathcal{H}_Q$ , may be much stronger than the amplitude of the rf excitation pulse. As a result, it affects the line intensity and alters the lineshape. These effects make the interpretation of spectra more difficult. Usually, only the first two expansion terms of  $\mathcal{H}_Q$  are considered: the first-order, ( $H_Q^{[1]}$ ), and second-order, ( $H_Q^{[2]}$ ), quadrupolar interactions, in the vocabulary of standard perturbation theory.  $H_Q^{[1]}$  splits the spectrum of a half-integer quadrupole spin system in a single crystal into  $2I - 1$  satellite lines, but the central line remains at the Larmor frequency  $\omega_0$ . The additional effect of  $H_Q^{[2]}$  is to shift further all the lines, including the central line.

When the sample is in powder form, as it usually is, it is mainly the central line that is observed. Moreover, its lineshape becomes nonsymmetrical when  $H_Q^{[2]}$  is large. In favorable cases, the powder pattern of the satellite spinning sidebands is detected using the popular MAS technique (see *Magic Angle Spinning* and *Rotating Solids*). The powder pattern of the central line is characterized by three parameters: the quadrupolar coupling constant  $\chi = e^2qQ/\hbar$ , which is the product of a nuclear property ( $eQ$ ) and a crystal property ( $eq$ ), the asymmetry parameter  $\eta$  and the center of gravity of the experimental line,  $\delta_{CG}^{exp}$  (in ppm).  $\chi$  is a measure of the strength of the quadrupolar interaction and  $\eta$  a measure of the deviation of the EFG from axial symmetry. The true chemical shift  $\delta_{CS}$

of the central line is related to these three parameters:<sup>1,2</sup>

$$\delta_{CS} = \delta_{CG}^{exp} + \frac{1}{30} \left( 1 + \frac{1}{3}\eta^2 \right) \left[ I(I+1) - \frac{3}{4} \right] \left[ \frac{3\chi}{2I(2I-1)\omega_0} \right]^2 \quad (1)$$

A precise determination of  $\delta_{CS}$  is required if its value has to be correlated with bond lengths and bond angles. Several methods are available for determining  $\chi$  and  $\eta$ . They can be grouped into two categories:

1. there is a series of techniques, especially the mechanical spinning of the sample,<sup>1–5</sup> based on the frequency domain response of the spin system (see *Variable Angle Sample Spinning*, *Satellite Transition NMR Spectroscopy of Half-Integer Quadrupolar Nuclei under Magic-Angle Spinning* and *Double Rotation NMR*);
2. the second series deals with the time domain response of the spin system to rf excitation<sup>6–8</sup> (see *Nutation Spectroscopy of Quadrupolar Nuclei*, *MQMAS NMR: Experimental Strategies and Applications* and *Advances in STMAS*).

The experimental center of gravity  $\delta_{CG}^{exp}$  is determined by spectral simulation. However, spectra acquired with DAS or DOR probes provide this value directly<sup>5</sup> (see *Double Rotation* and *Dynamic Angle Spinning*). Books dealing with these modern techniques are available.<sup>9–11</sup>

In the present article, we focus on the frequency domain response of half-integer quadrupolar spin larger than 1. (Jellison and co-workers<sup>12</sup> calculated perturbation terms up to third order for integer spins  $I = 1$  and 3.) The first part is devoted to a derivation of the Hamiltonians corresponding to first- and second-order perturbations, with the emphasis on the different conventions used in the literature, namely, the asymmetry parameter, the components of spherical tensors in their principal axis system, the Larmor frequency, transitions, and the transition frequency. With this in mind, the Magnus expansion is applied instead of standard perturbation theory. For simplicity, Hamiltonians are expressed in angular velocity units and relaxation phenomena are not taken into account. In the second part, NMR parameters related to single crystal spectra (see *High-Pressure NMR*, *Incommensurate Systems*, and *Phase Transitions and Critical Phenomena in Solids*) and powder patterns in static and MAS measurements are presented (see *Amorphous Materials*, *Quadrupolar Nuclei in Glasses*, *Quadrupolar Nuclei in Liquid Samples*, *Vanadium Catalysts: Solid State NMR*, *Massiot, Dominique: Materials by NMR of Quadrupoles from Room to High Temperature*, *Chlorine, Bromine, and Iodine Solid-State NMR* and *Quadrupolar NMR in Earth Sciences*), in particular, the second-order quadrupolar shift, the critical points and the lineshapes of the powder patterns for various values of  $\eta$ , and the second-order quadrupolar shift for the center of gravity of a powder pattern. In the appendix, the commonly used Euler angles as well as those used by Baugher and co-workers<sup>13–15</sup> are given in graphical form. The Wigner rotation matrix, expressing the components of the same spherical tensor in two different coordinate frames, is also given.

**Table 1** Value of nuclear spin  $I$  as a function of atomic number  $Z$  and mass number  $A$ 

A	Z	
	Odd	Even
Odd	Half-integer $I$	Half-integer $I$
Even	Integer $I$	$I = 0$

## 2 QUADRPOLAR HAMILTONIAN IN A UNIFORM SPACE

Slichter<sup>16</sup> and others<sup>17,18</sup> introduce the quadrupolar interaction from the classical concept of the charge density for a nucleus in a space where the three coordinate axes  $x$ ,  $y$ , and  $z$  are equivalent. Then, the quantum mechanical form of this interaction is obtained using operators. Thanks to the Wigner–Eckart theorem, the Hamiltonian representing the quadrupolar interaction independently of the Cartesian coordinate frame is defined:

$$\hbar\hat{\mathcal{H}}_Q = \frac{eQ}{6I(2I-1)} \sum_{\alpha,\beta=x,y,z} V_{\alpha\beta} [\frac{3}{2}(\hat{I}_\alpha\hat{I}_\beta + \hat{I}_\beta\hat{I}_\alpha) - \delta_{\alpha\beta}I(I+1)] \quad (2a)$$

with

$$V_{\alpha\beta} = \left. \frac{\partial^2 U}{\partial\alpha\partial\beta} \right|_{r=0} \quad (2b)$$

$\delta_{\alpha\beta}$  is the Kronecker delta symbol,  $U$  is the electrostatic potential at the origin (inside the nucleus) generated by external charges, and  $V_{\alpha\beta}$  are the Cartesian components of the EFG at the origin,  $\mathbf{V}$ , which is a second-rank symmetrical tensor (see *Deuterium NMR in Solids, Liquid Crystalline Samples: Deuterium NMR* and *Membranes: Deuterium NMR*). In the principal axis system  $\Sigma^{\text{PAS}}$  of the EFG,  $\mathbf{V}$  is diagonal:

$$\mathbf{V} = \begin{bmatrix} V_{XX} & 0 & 0 \\ 0 & V_{YY} & 0 \\ 0 & 0 & V_{ZZ} \end{bmatrix} \quad (3)$$

with the convention  $|V_{ZZ}| \geq |V_{YY}| \geq |V_{XX}|$ . Furthermore, the Laplace equation  $V_{XX} + V_{YY} + V_{ZZ} = 0$  holds for  $\mathbf{V}$ . Thus, only two independent parameters are required:

$$eq = V_{ZZ} \quad (4a)$$

$$\eta = \frac{V_{XX} - V_{YY}}{V_{ZZ}} \quad (4b)$$

the largest component and the asymmetry parameter, respectively, with  $1 \geq \eta \geq 0$ .

In the coordinate frame  $\Sigma^{\text{PAS}}$ , the Cartesian tensor representation of the quadrupolar interaction [equation (2a)] takes the form

$$\hbar\hat{\mathcal{H}}_Q = \frac{e^2qQ}{4I(2I-1)} [3\hat{I}_Z^2 - I(I+1) + \eta(\hat{I}_X^2 - \hat{I}_Y^2)] \quad (5a)$$

In terms of the operators

$$\hat{I}_+ = \hat{I}_X + i\hat{I}_Y, \quad \hat{I}_- = \hat{I}_X - i\hat{I}_Y \quad (5b)$$

equation (5a) becomes

$$\hbar\hat{\mathcal{H}}_Q = \frac{e^2qQ}{4I(2I-1)} [3\hat{I}_Z^2 - I(I+1) + \frac{1}{2}\eta(\hat{I}_+^2 + \hat{I}_-^2)] \quad (5c)$$

Sometimes, the opposite convention is adopted for  $\eta$ :

$$\eta = \frac{V_{YY} - V_{XX}}{V_{ZZ}} \quad (6)$$

which is associated with the condition  $|V_{ZZ}| \geq |V_{XX}| \geq |V_{YY}|$ .<sup>19,20</sup> As a result, a negative sign appears in front of  $\eta$  in equations (5a) and (5c) and in subsequent expressions containing  $\eta$ .

## 3 SPHERICAL TENSOR REPRESENTATION FOR THE QUADRPOLAR HAMILTONIAN

The passage from one coordinate frame to another is more conveniently realized if the quadrupolar interaction is expressed as a second-rank irreducible spherical tensor (see *Internal Spin Interactions and Rotations in Solids and Tensors in NMR*), according to Mehring:<sup>21</sup>

$$\begin{aligned} \hbar\hat{\mathcal{H}}_Q &= \frac{eQ}{2I(2I-1)} \sum_{q=-2}^2 (-1)^q V^{(2,q)} T^{(2,-q)} \\ &= \frac{eQ}{2I(2I-1)} \sum_{q=-2}^2 (-1)^q V^{(2,-q)} T^{(2,q)} \end{aligned} \quad (7)$$

In any Cartesian coordinate frame  $\Sigma$ , the spherical tensor and Cartesian tensor components of  $\mathbf{V}$  are related by

$$\left. \begin{aligned} V^{(2,0)} &\equiv V_0 = 3\sqrt{\frac{1}{6}}V_{zz} \\ V^{(2,1)} &\equiv V_1 = -V_{xz} - iV_{yz} \\ V^{(2,-1)} &\equiv V_{-1} = V_{xz} - iV_{yz} \\ V^{(2,2)} &\equiv V_2 = \frac{1}{2}(V_{xx} - V_{yy}) + iV_{xy} \\ V^{(2,-2)} &\equiv V_{-2} = \frac{1}{2}(V_{xx} - V_{yy}) - iV_{xy} \end{aligned} \right\} \quad (8)$$

and those of  $\mathbf{T}$  as

$$\left. \begin{aligned} T^{(2,0)} &= \frac{1}{6}\sqrt{6}[3\hat{I}_z^2 - I(I+1)] \\ T^{(2,1)} &= -\frac{1}{2}(\hat{I}_z\hat{I}_+ + \hat{I}_+\hat{I}_z) \\ T^{(2,-1)} &= \frac{1}{2}(\hat{I}_z\hat{I}_- + \hat{I}_-\hat{I}_z) \\ T^{(2,2)} &= \frac{1}{2}\hat{I}_+\hat{I}_+ \\ T^{(2,-2)} &= \frac{1}{2}\hat{I}_-\hat{I}_- \end{aligned} \right\} \quad (9)$$

with  $\hat{I}_+ = \hat{I}_x + i\hat{I}_y$  and  $\hat{I}_- = \hat{I}_x - i\hat{I}_y$ . These two operators are different from those of equation (5b) despite the same notation. It is worth noting that the numerical factors in the components of  $\mathbf{V}$  and  $\mathbf{T}$  [equations (8) and (9)] differ from author to author.

Using equations (7)–(9), the spherical tensor representation of the quadrupolar interaction in the coordinate frame  $\Sigma$  becomes

$$\begin{aligned} \hbar\hat{\mathcal{H}}_Q &= \frac{eQ}{4I(2I-1)} \{ \frac{1}{3}\sqrt{6}[3\hat{I}_z^2 - I(I+1)]V_0 \\ &\quad + (\hat{I}_z\hat{I}_+ + \hat{I}_+\hat{I}_z)V_{-1} \\ &\quad - (\hat{I}_z\hat{I}_- + \hat{I}_-\hat{I}_z)V_1 + \hat{I}_+^2V_{-2} + \hat{I}_-^2V_2 \} \end{aligned} \quad (10)$$

Slichter<sup>16</sup> uses nearly the same relationship, apart from a negative sign due to another choice of  $V_1$ . From equations (4a), (4b), and (8), the spherical tensor components of  $\mathbf{V}$  in

$\Sigma^{\text{PAS}}$  are obtained:

$$\begin{aligned} V_0^{\text{PAS}} &= \sqrt{\frac{3}{2}}eq, & V_1^{\text{PAS}} &= V_{-1}^{\text{PAS}} = 0, \\ V_2^{\text{PAS}} &= V_{-2}^{\text{PAS}} = \frac{1}{2}eq\eta \end{aligned} \quad (11a)$$

If the other convention for  $\eta$ , namely, equation (6) is used then the spherical tensor components of  $\mathbf{V}$  in  $\Sigma^{\text{PAS}}$  are<sup>20</sup>

$$\begin{aligned} V_0^{\text{PAS}} &= \sqrt{\frac{3}{2}}eq, & V_1^{\text{PAS}} &= V_{-1}^{\text{PAS}} = 0, \\ V_2^{\text{PAS}} &= V_{-2}^{\text{PAS}} = -\frac{1}{2}eq\eta \end{aligned} \quad (11b)$$

#### 4 QUADROPOLAR INTERACTION AS A PERTURBATION OF ZEEMAN INTERACTION

A nuclear spin possesses a magnetic moment  $\boldsymbol{\mu}$  and an angular momentum  $\hbar\mathbf{I}$ , which are related by the gyromagnetic ratio  $\gamma$ :

$$\boldsymbol{\mu} = \gamma\hbar\mathbf{I} \quad (12)$$

In the laboratory frame  $\Sigma^{\text{lab}}$ , the direction of the strong static magnetic field  $\mathbf{B}_0$  is taken as the  $z$  axis. The coupling of the magnetic moment with  $\mathbf{B}_0$  is the Zeeman interaction  $\hat{\mathcal{H}}_Z$ :

$$\hbar\hat{\mathcal{H}}_Z = -\boldsymbol{\mu} \cdot \mathbf{B}_0 = -\hbar\omega_0\hat{I}_z \quad (13a)$$

$$\omega_0 = \gamma B_0 \quad (13b)$$

where  $\omega_0/2\pi$  is the Larmor frequency. Sometimes this frequency is defined as  $\omega_0/2\pi = -\gamma B_0/2\pi$ . As a result, the Zeeman interaction takes the form  $\hbar\hat{\mathcal{H}}_Z = \hbar\omega_0\hat{I}_z$ . As with  $\eta$ , the choice of  $\omega_0$  changes the sign of some expressions below.

We deal with the case where  $\mathcal{H}_Q$  can be treated as a weak perturbation of the Zeeman interaction. It is then more convenient to express interactions in the frame  $\Sigma^{\text{obs}}$  rotating relative to  $\Sigma^{\text{lab}}$  with an angular velocity  $\omega_0$  so that the spherical tensor representation of the quadrupolar interaction expressed by equation (10) becomes time-dependent:<sup>22</sup>

$$\begin{aligned} \hbar\hat{\mathcal{H}}_Q(t) &= \exp(i\hat{\mathcal{H}}_Z t)\hbar\hat{\mathcal{H}}_Q \exp(-i\hat{\mathcal{H}}_Z t) \\ &= \frac{eQ}{4I(2I-1)} \left\{ \frac{1}{3}\sqrt{6}[3\hat{I}_z^2 - I(I+1)]V_0 \right. \\ &\quad + \hat{I}_+(2\hat{I}_z + 1)V_{-1} \exp(-i\omega_0 t) \\ &\quad - \hat{I}_-(2\hat{I}_z - 1)V_1 \exp(i\omega_0 t) \\ &\quad \left. + \hat{I}_+^2 V_{-2} \exp(-i2\omega_0 t) + \hat{I}_-^2 V_2 \exp(i2\omega_0 t) \right\} \quad (14) \end{aligned}$$

However, the first term in the curly brackets (i.e., the secular term) remains time-independent. In order to make the quadrupolar interaction completely time-independent,  $\hat{\mathcal{H}}_Q(t)$  is averaged over one Larmor period  $2\pi/\omega_0$  up to first-order (see *Average Hamiltonian Theory*), using the Magnus expansion:<sup>23</sup>

$$\begin{aligned} \langle \hat{\mathcal{H}}_Q(t) \rangle &= \frac{\omega_0}{2\pi} \int_0^{2\pi/\omega_0} dt \hat{\mathcal{H}}_Q(t) - \frac{i\omega_0}{4\pi} \int_0^{2\pi/\omega_0} dt \int_0^t \\ &\quad \times dt' [\hat{\mathcal{H}}_Q(t), \hat{\mathcal{H}}_Q(t')] = H_Q^{(0)} + H_Q^{(1)} \end{aligned} \quad (15)$$

with

$$H_Q^{(0)} = \frac{eQ}{4I(2I-1)\hbar} \frac{\sqrt{6}}{3} [3\hat{I}_z^2 - I(I+1)]V_0 \quad (16)$$

$$\begin{aligned} H_Q^{(1)} &= -\frac{1}{\omega_0} \left[ \frac{eQ}{4I(2I-1)\hbar} \right]^2 \left\{ \sqrt{6}V_0V_{-1}\hat{I}_+(2\hat{I}_z + 1)^2 \right. \\ &\quad - \sqrt{6}V_0V_1\hat{I}_-(2\hat{I}_z - 1)^2 + 2\sqrt{6}V_0V_{-2}\hat{I}_+^2(\hat{I}_z + 1) \\ &\quad + 2\sqrt{6}V_0V_2\hat{I}_-^2(\hat{I}_z - 1) \\ &\quad + 2V_{-1}V_1\hat{I}_z[4I(I+1) - 8\hat{I}_z^2 - 1] \\ &\quad \left. + 2V_{-2}V_2\hat{I}_z[2I(I+1) - 2\hat{I}_z^2 - 1] \right\} \quad (17) \end{aligned}$$

Usually, only the secular terms that commute with  $\hat{I}_z$  (i.e., the last two terms in the curly brackets of  $H_Q^{(1)}$ ) are considered.

With this simplification,  $H_Q^{(0)}$  and  $H_Q^{(1)}$  are equivalent to the first-order,  $H_Q^{[1]}$ , and second-order,  $H_Q^{[2]}$ , terms in standard perturbation theory,<sup>24</sup> i.e.,

$$H_Q^{[1]} = H_Q^{(0)} = \frac{eQ}{4I(2I-1)\hbar} \frac{\sqrt{6}}{3} [3\hat{I}_z^2 - I(I+1)]V_0 \quad (18)$$

$$\begin{aligned} H_Q^{[2]} = H_Q^{(1)} &= -\frac{1}{\omega_0} \left[ \frac{eQ}{4I(2I-1)\hbar} \right]^2 \\ &\quad \times \{ 2V_{-1}V_1\hat{I}_z[4I(I+1) - 8\hat{I}_z^2 - 1] \\ &\quad + 2V_{-2}V_2\hat{I}_z[2I(I+1) - 2\hat{I}_z^2 - 1] \} \quad (19) \end{aligned}$$

respectively. Equations (18) and (19), derived in the rotating frame  $\Sigma^{\text{obs}}$ , are unchanged in the laboratory frame  $\Sigma^{\text{lab}}$ . This is because they commute with the Zeeman interaction. In other words, they commute with the operator  $\hat{I}_z$ . From now on, we shall use the language of standard perturbation theory. The first-order quadrupolar interaction  $H_Q^{[1]}$  is independent of  $\omega_0$ , whereas the second-order quadrupolar interaction  $H_Q^{[2]}$  is inversely proportional to  $\omega_0$ . Therefore, a strong static magnetic field is required to reduce the effects of  $H_Q^{[2]}$ .

#### 5 ENERGY LEVELS AND THE SPECTRUM OF A SINGLE CRYSTAL

When a free spin  $I$  is introduced into a strong static magnetic field, the Zeeman interaction splits its  $2I+1$  energy levels  $|m\rangle$ , whose energy is defined by

$$\langle m|\hat{\mathcal{H}}_Z|m\rangle = -m\omega_0 \quad (20)$$

and the difference between two consecutive energy levels ( $m-1, m$ ), expressed in angular velocity units, is

$$\omega_{m-1,m}^{(Z)} = \langle m-1|\hat{\mathcal{H}}_Z|m-1\rangle - \langle m|\hat{\mathcal{H}}_Z|m\rangle = \omega_0 \quad (21a)$$

We choose the same convention as Abragam<sup>18</sup> for the pair ( $m-1, m$ ) and equation (21a) to represent the transition and the transition frequency, respectively, but other authors choose ( $m, m-1$ ), ( $m, m+1$ ), ( $m+1, m$ ), equation (21a) or its negative

$$\omega_{m-1,m}^{(Z)} = \langle m|\hat{\mathcal{H}}_Z|m\rangle - \langle m-1|\hat{\mathcal{H}}_Z|m-1\rangle \quad (21b)$$

Of course, these choices affect some later relationships dealing with transitions and transition frequencies. Equation (21a) implies that the energy levels  $|m\rangle$  of a free spin in a strong static magnetic field  $\mathbf{B}_0$  are equally spaced. The separation between two adjacent levels is  $\omega_0$ . In the spectrum, a single line is located at  $\omega_0$ . However, these energy levels may be shifted by other interactions, including the quadrupolar interaction discussed in this article.

The first-order quadrupolar interaction  $H_Q^{[1]}$  shifts the energy levels  $|m\rangle$  by an amount

$$\langle m|H_Q^{[1]}|m\rangle = \frac{eQ}{4I(2I-1)\hbar} \frac{\sqrt{6}}{3} [3m^2 - I(I+1)]V_0 \quad (22)$$

and in the spectrum, its contribution to the line position, i.e., the first-order quadrupolar shift  $\omega_{m-1,m}^{(1)}$  of the line position associated with the transition  $(m-1, m)$ , is

$$\begin{aligned} \omega_{m-1,m}^{(1)} &= \langle m-1|H_Q^{[1]}|m-1\rangle - \langle m|H_Q^{[1]}|m\rangle \\ &= \frac{3eQ}{4I(2I-1)\hbar} \frac{\sqrt{6}}{3} (1-2m)V_0 \end{aligned} \quad (23)$$

The spectrum consists of  $2I$  lines, the central one of which, associated with the transition  $(-\frac{1}{2}, \frac{1}{2})$ , is still located at  $\omega_0$ . The other  $2I-1$  lines are called satellite lines.

When the second-order quadrupolar interaction  $H_Q^{[2]}$  is taken into account, the energy levels  $|m\rangle$  are shifted further:<sup>25</sup>

$$\begin{aligned} \langle m|H_Q^{[2]}|m\rangle &= -\frac{1}{\omega_0} \left[ \frac{eQ}{4I(2I-1)\hbar} \right]^2 \\ &\quad \times \{2V_{-1}V_1m[4I(I+1) - 8m^2 - 1] \\ &\quad + 2V_{-2}V_2m[2I(I+1) - 2m^2 - 1]\} \end{aligned} \quad (24)$$

and its contribution  $\omega_{m-1,m}^{(2)}$  to the line position, i.e., the second-order quadrupolar shift of the line, is<sup>26</sup>

$$\begin{aligned} \omega_{m-1,m}^{(2)} &= \langle m-1|H_Q^{[2]}|m-1\rangle - \langle m|H_Q^{[2]}|m\rangle \\ &= -\frac{2}{\omega_0} \left[ \frac{eQ}{4I(2I-1)\hbar} \right]^2 \\ &\quad \times \{V_{-1}V_1[24m(m-1) - 4I(I+1) + 9] \\ &\quad + \frac{1}{2}V_{-2}V_2[12m(m-1) - 4I(I+1) + 6]\} \end{aligned} \quad (25)$$

Therefore, the line associated with the transition  $(m-1, m)$  is located in the spectrum at

$$\omega_{m-1,m} = \omega_0 + \omega_{m-1,m}^{(1)} + \omega_{m-1,m}^{(2)} \quad (26)$$

In the following two subsections, we apply equation (26) to two experiments, in which the single crystal is either static or is spinning at the magic angle.

### 5.1 Spectrum of a Static Single Crystal

We have to express  $V_0$  in equation (23), and  $V_1$ ,  $V_{-1}$ ,  $V_2$ , and  $V_{-2}$  in equation (25) in terms of the components of  $\mathbf{V}$  in  $\Sigma^{\text{PAS}}$ , equation (11a). For this purpose, the following relationship is used:

$$V_i = \sum_{j=-2}^2 \mathcal{D}_{j,i}^{(2)}(\alpha, \beta, \gamma) V_j^{\text{PAS}} \quad (27)$$

where the Euler angles  $\alpha$ ,  $\beta$ , and  $\gamma$  describe the direction of the strong static magnetic field in  $\Sigma^{\text{PAS}}$  (Figure 1) and  $\mathcal{D}_{j,i}^{(2)}(\alpha, \beta, \gamma)$  is the Wigner rotation matrix defined in the appendix. For example,

$$V_0 = \sqrt{\frac{3}{2}} eQ \left[ \frac{1}{2}(3 \cos^2 \beta - 1) + \frac{1}{2}\eta \sin^2 \beta \cos 2\alpha \right] \quad (28)$$

Its substitution into equation (18) yields

$$H_Q^{[1]} = \frac{1}{3}\omega_Q [3\hat{I}_z^2 - I(I+1)] \quad (29)$$

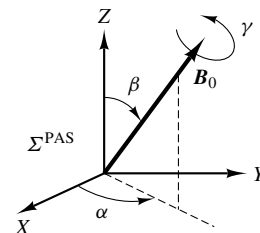


**Figure 1** Euler angles defining the direction of  $\mathbf{B}_0$  in the principal axis system  $\Sigma^{\text{PAS}}$  of the EFG during a static experiment

with

$$\omega_Q = \frac{3\chi}{4I(2I-1)} \left[ \frac{1}{2}(3 \cos^2 \beta - 1) + \frac{1}{2}\eta \sin^2 \beta \cos 2\alpha \right] \quad (30)$$

A negative sign will appear in front of  $\eta$  if the other convention for  $\eta$ , equation (6), is chosen or the Euler angles used by Baugher and co-workers<sup>13-15</sup> are used. The definitions of  $H_Q^{[1]}$  by equation (29) or of  $\omega_Q$  by equation (30) are not unique. Other definitions can be found in the literature. The first-order quadrupolar shift of the lines  $(m-1, m)$ , equation (23), becomes

$$\omega_{m-1,m}^{(1)\text{static}} = (1-2m)\omega_Q \quad (31)$$

The lines in the spectrum are separated by the same quantity  $2\omega_Q$ , but the central line is not shifted.

The other two factors  $V_1V_{-1}$  and  $V_2V_{-2}$  in equation (25) are

$$\begin{aligned} 2V_1V_{-1} &= -\frac{3}{2}e^2q^2 \left[ \left(-\frac{1}{3}\eta^2 \cos^2 2\alpha + 2\eta \cos 2\alpha - 3\right) \cos^4 \beta \right. \\ &\quad \left. + \left(\frac{2}{3}\eta^2 \cos^2 2\alpha - 2\eta \cos 2\alpha - \frac{1}{3}\eta^2 + 3\right) \cos^2 \beta \right. \\ &\quad \left. + \frac{1}{3}\eta^2(1 - \cos^2 2\alpha) \right] \end{aligned} \quad (32a)$$

$$\begin{aligned} V_2V_{-2} &= \frac{3}{2}e^2q^2 \left[ \left(\frac{1}{24}\eta^2 \cos^2 2\alpha - \frac{1}{4}\eta \cos 2\alpha + \frac{3}{8}\right) \cos^4 \beta \right. \\ &\quad \left. + \left(-\frac{1}{12}\eta^2 \cos^2 2\alpha + \frac{1}{6}\eta^2 - \frac{3}{4}\right) \cos^2 \beta \right. \\ &\quad \left. + \frac{1}{24}\eta^2 \cos^2 2\alpha + \frac{1}{4}\eta \cos 2\alpha + \frac{3}{8} \right] \end{aligned} \quad (32b)$$

The second-order quadrupolar shift of the central line, using equation (25), is given by

$$\begin{aligned} \omega_{-1/2,1/2}^{(2)\text{static}} &= -\frac{1}{6\omega_0} \left[ \frac{3\chi}{2I(2I-1)} \right]^2 \left[ I(I+1) - \frac{3}{4} \right] \\ &\quad \times [A(\alpha, \eta) \cos^4 \beta + B(\alpha, \eta) \cos^2 \beta + C(\alpha, \eta)] \end{aligned} \quad (33)$$

with

$$\left. \begin{aligned} A(\alpha, \eta) &= -\frac{27}{8} + \frac{9}{4}\eta \cos 2\alpha - \frac{3}{8}(\eta \cos 2\alpha)^2 \\ B(\alpha, \eta) &= \frac{30}{8} - \frac{1}{2}\eta^2 - 2\eta \cos 2\alpha + \frac{3}{4}(\eta \cos 2\alpha)^2 \\ C(\alpha, \eta) &= -\frac{3}{8} + \frac{1}{3}\eta^2 - \frac{1}{4}\eta \cos 2\alpha - \frac{3}{8}(\eta \cos 2\alpha)^2 \end{aligned} \right\} \quad (34)$$

When the EFG has axial symmetry ( $\eta = 0$ ), equation (33) becomes simply

$$\begin{aligned} \omega_{-1/2,1/2}^{(2)\text{static}} &= -\frac{1}{16\omega_0} \left[ \frac{3\chi}{2I(2I-1)} \right]^2 \left[ I(I+1) - \frac{3}{4} \right] \\ &\quad \times (1 - \cos^2 \beta)(9 \cos^2 \beta - 1) \end{aligned} \quad (35)$$

It is worth noting that the third Euler angle  $\gamma$  does not appear in equations (30), (33), and (34); this is because  $\mathbf{B}_0$  is a symmetry axis for the spins. Our results are identical

to those of Narita and co-workers<sup>27</sup> [note that their paper contains a typographical error concerning the expression of  $\cos 2\alpha$  in  $C(\alpha, \eta)$ ]. Subsequently, Baugher and co-workers<sup>15</sup> obtained expressions similar to equation (34), except that their terms containing  $\eta$  have the opposite sign. Their comment 23, concerning the sign in front of all the terms in  $\cos 2\alpha$ , is explained in our appendix using the Euler angles (Figure 10) defined by Goldstein.<sup>14</sup> Another way to obtain the same results as those of Baugher and co-workers<sup>15</sup> is to employ the usual Euler angles (Figure 9) and to replace  $\eta$  by  $-\eta$  (the other convention for  $\eta$ ). This point is confirmed by Hirshinger and co-workers<sup>28</sup> and by Chu and Gerstein.<sup>29</sup> Wolf and co-workers<sup>30</sup> have determined the third-order perturbation term, and shown that it is proportional to  $(2m-1)/\omega_0^2$ . Therefore, the position of the central line is not shifted further by this new term.

## 5.2 Spectrum of a Rotating Single Crystal

First of all, the expressions for  $V_0, V_1, V_{-1}, V_2,$  and  $V_{-2}$  must be expressed in terms of the components of  $\mathbf{V}$  in the coordinate frame  $\Sigma^{\text{MAS}}$  of the rotor. To do this, the Wigner rotation matrix is applied once more:

$$V_i = \sum_{j=-2}^2 \mathcal{D}_{j,i}^{(2)}(\omega_r t, \theta_m, 0) V_j^{\text{MAS}} \quad (36)$$

where  $\omega_r$  is the angular velocity of the rotor and  $\theta_m = 54.73^\circ$  is the magic angle (Figure 2). Then,  $V_j^{\text{MAS}}$  must be expressed in terms of the components of  $\mathbf{V}$  in  $\Sigma^{\text{PAS}}$ :

$$V_j^{\text{MAS}} = \sum_{k=-2}^2 \mathcal{D}_{k,j}^{(2)}(\alpha, \beta, \gamma) V_k^{\text{PAS}} \quad (37)$$

where the Euler angles  $\alpha, \beta,$  and  $\gamma$  describe the direction of the rotor in  $\Sigma^{\text{PAS}}$  (Figure 3).

The first step, equation (36), yields

$$\omega_{m-1,m}^{(1)\text{MAS}} = \sqrt{\frac{2}{3}}(1-2m) \frac{3eQ}{8I(2I-1)\hbar} V_0^{\text{MAS}} (3\cos^2\theta_m - 1) \quad (38)$$

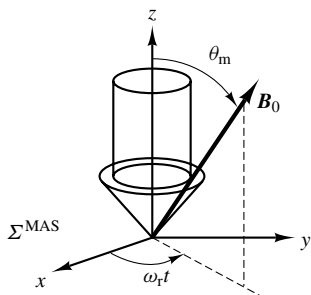


**Figure 2** Euler angles defining the direction of  $\mathbf{B}_0$  in the rotor coordinate frame  $\Sigma^{\text{MAS}}$  during a MAS experiment. In  $\Sigma^{\text{MAS}}$ ,  $\mathbf{B}_0$  rotates around the rotor with the angular velocity  $\omega_r$ ;  $\theta_m$  is the magic angle; the third angle is  $\gamma = 0$ .  $\mathbf{B}_0$  performs a right-hand, positive rotation in  $\Sigma^{\text{MAS}}$ . Therefore, the rotor performs a right-hand, negative rotation in  $\Sigma^{\text{lab}}$ .

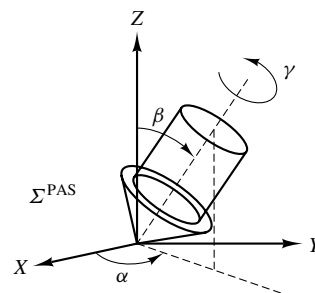


**Figure 3** Euler angles defining the direction of the rotor in the principal axis system  $\Sigma^{\text{PAS}}$  of the EFG during a MAS experiment. In  $\Sigma^{\text{PAS}}$ , the rotor containing the sample appears static

The second step, equation (37), yields the first-order quadrupolar shift:

$$\omega_{m-1,m}^{(1)\text{MAS}} = \frac{1}{2}(1-2m)\omega_Q(3\cos^2\theta_m - 1) \quad (39)$$

This shift is zero when the crystal rotates at the magic angle. In other words, all the energy levels become equally spaced. Therefore, a single line instead of  $2I$  lines appears in the spectrum at  $\omega_0$ .

For the second-order quadrupolar shift, the first step, equation (36), yields

$$\begin{aligned} \omega_{m-1,m}^{(2)\text{MAS}} = & -\frac{2}{\omega_0} \left[ \frac{eQ}{4I(2I-1)\hbar} \right]^2 \\ & \times \left\{ -\frac{1}{6} V_2^{\text{MAS}} V_{-2}^{\text{MAS}} [50m(m-1) - 6I(I+1) + 17] \right. \\ & + \frac{1}{3} V_1^{\text{MAS}} V_{-1}^{\text{MAS}} [8m(m-1) + 2] \\ & \left. - \frac{1}{2} V_0^{\text{MAS}} V_0^{\text{MAS}} [14m(m-1) - 2I(I+1) + 5] \right\} \quad (40) \end{aligned}$$

The second step, equation (37), yields, in the fast rotation regime,<sup>1</sup>

$$\begin{aligned} \omega_{m-1,m}^{(2)\text{MAS}} = & -\frac{3}{32\omega_0} \left[ \frac{\chi}{I(2I-1)} \right]^2 (1 + \frac{1}{3}\eta^2) \\ & \times [2I(I+1) - 14m(m-1) - 5] \\ & + \frac{3}{128\omega_0} \left[ \frac{\chi}{I(2I-1)} \right]^2 \\ & \times [6I(I+1) - 34m(m-1) - 13]g(\alpha, \beta, \eta) \quad (41) \end{aligned}$$

with

$$\begin{aligned} g(\alpha, \beta, \eta) = & \frac{1}{2}(1 + 6\cos^2\beta - 7\cos^4\beta) \\ & + \frac{1}{3}\eta(1 - 8\cos^2\beta + 7\cos^4\beta)\cos 2\alpha \\ & + \frac{1}{18}\eta^2[-7(1 - \cos^2\beta)^2\cos^2 2\alpha + 8 - 4\cos^2\beta] \quad (42) \end{aligned}$$

For the central line, the second-order quadrupolar shift is<sup>31</sup>

$$\begin{aligned} \omega_{-1/2,1/2}^{(2)\text{MAS}} = & -\frac{1}{6\omega_0} \left[ \frac{3\chi}{2I(2I-1)} \right]^2 [I(I+1) - \frac{3}{4}] \\ & \times [D(\alpha, \eta)\cos^4\beta + E(\alpha, \eta)\cos^2\beta + F(\alpha, \eta)] \quad (43) \end{aligned}$$

with

$$\left. \begin{aligned} D(\alpha, \eta) &= \frac{21}{16} - \frac{7}{8}\eta \cos 2\alpha + \frac{7}{48}(\eta \cos 2\alpha)^2 \\ E(\alpha, \eta) &= -\frac{9}{8} + \frac{1}{12}\eta^2 + \eta \cos 2\alpha - \frac{7}{24}(\eta \cos 2\alpha)^2 \\ F(\alpha, \eta) &= \frac{5}{16} - \frac{1}{8}\eta \cos 2\alpha + \frac{7}{48}(\eta \cos 2\alpha)^2 \end{aligned} \right\} (44)$$

As in the case of a static sample, the Euler angle  $\gamma$  does not appear in equations (43) and (44). This is because the experimental conditions correspond to the fast rotation regime. However, this angle does appear in the intermediate regime where the angular velocity of the rotor is of the same order of magnitude as the linewidth. As a result, spinning sidebands appear in the spectrum. Samoson and co-workers<sup>23</sup> established a general expression for  $\Omega_{m-1,m}^{(2)MAS}$  that clearly shows the presence of modulations due to the rotation of the rotor:

$$\Omega_{m-1,m}^{(2)MAS} = \omega_{m-1,m}^{(2)MAS} + \sum_{n=1}^4 [A_n \cos(n\omega_r t) + B_n \sin(n\omega_r t)] \quad (45)$$

Two typographical errors appear in the *annexe* of their paper:<sup>23</sup> the expressions for  $A_1^\lambda$  and  $A_2^\lambda$  should be

$$\left. \begin{aligned} A_1^\lambda &= -\frac{1}{2}\sqrt{2} \sin 2\beta^\lambda \rho_{20}^\lambda + \frac{1}{3}\sqrt{3} \cos 2\alpha^\lambda \sin 2\beta^\lambda \rho_{22}^\lambda \\ A_2^\lambda &= \frac{1}{2} \sin^2 \beta^\lambda \rho_{20}^\lambda + \frac{1}{6}\sqrt{6} \cos 2\alpha^\lambda (1 + \cos^2 \beta^\lambda) \rho_{22}^\lambda \end{aligned} \right\} (46)$$

Equation (45) allows us to investigate the spinning sidebands (see *High Speed MAS of Half-Integer Quadrupolar Nuclei in Solids, Sideband Analysis in Magic Angle Spinning NMR of Solids* and *Samoson, Ago: Development of High-Resolution NMR of Quadrupole Nuclei in Solids*).

## 6 POWDER SPECTRUM

In most cases, the sample is in powder form, because the growth of single crystals of significant size is not always possible. As a result, only the central line is detected in NMR (see *Fast Ion Conductors, Geological Applications, High Temperature Superconductors, Intercalation Compounds, Molecular Sieves: Crystalline Systems* and *Multiple-Quantum Magic-angle Spinning Experiments on Half-integer Nuclei: Fundamentals*). However, satellite lines can be detected without spinning the sample if  $\chi/2\pi < 300$  kHz; for example, for  $^{23}\text{Na}$  ( $I = \frac{3}{2}$ ) in  $\text{NaNO}_3$  or  $^7\text{Li}$  ( $I = \frac{3}{2}$ ) in  $\text{LiNbO}_3$ . When the MAS technique is applied, the spinning sidebands of the satellite lines are detected; for example, for iodine  $^{127}\text{I}$  ( $I = \frac{5}{2}$ ) in KI or the two isotopes of bromine ( $I = \frac{3}{2}$ ) in KBr. These two compounds are used for setting the magic angle of the MAS probe in the vicinity of  $^{29}\text{Si}$  and  $^{27}\text{Al}$  frequencies, respectively.

In a powder sample, the principal axes of the EFG associated with each crystallite are randomly oriented with respect to  $\mathbf{B}_0$ . The transition frequencies are not unique, but depend on the distribution of the Euler angles  $\alpha$  and  $\beta$  describing the direction of the rotor in the coordinate frame  $\Sigma^{\text{PAS}}$  in a MAS experiment at high spinning rate, or the direction of  $\mathbf{B}_0$  in the coordinate frame  $\Sigma^{\text{PAS}}$  in an experiment without spinning.

The resonance condition  $\omega(\alpha, \cos \beta)$  represents a surface in a three-dimensional space described by the parameters  $\omega$ ,  $\alpha$ , and  $\cos \beta$ . The critical points of this surface define divergences and shoulders in the spectrum. They are roots of the two

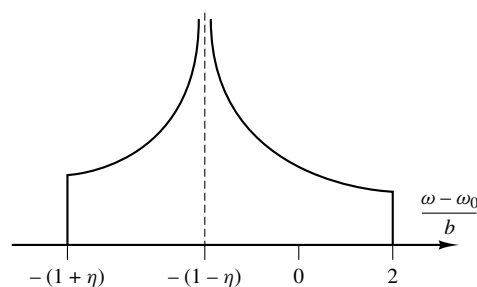


**Figure 4** Critical points<sup>13</sup> of a satellite powder pattern associated with the transition  $(m-1, m)$ ;  $b = 3\chi(1-2m)/8I(2I-1)$

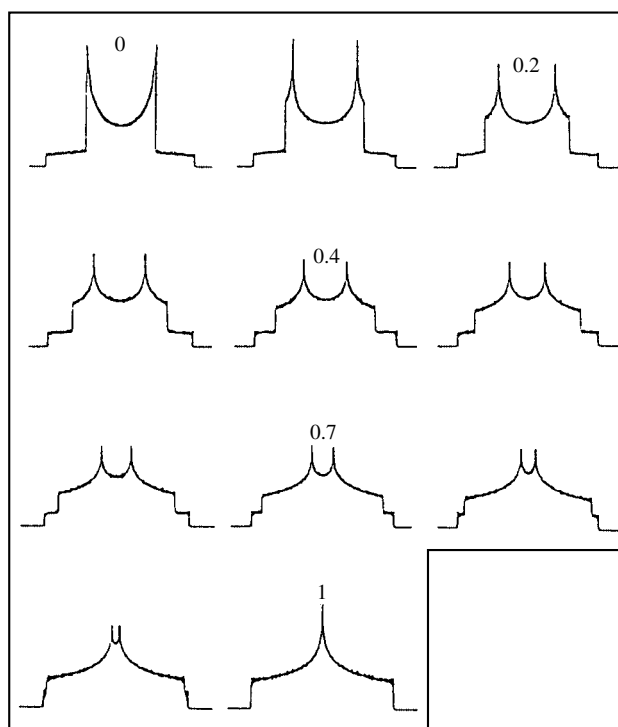


**Figure 5** Simulated powder pattern of a pair of satellite lines for increasing values of the asymmetry parameter  $\eta$  from 0 to 1 in steps of 0.1

coupled equations<sup>12,13</sup>

$$\left. \begin{aligned} \frac{\partial}{\partial \alpha} \omega(\alpha, \cos \beta) \Big|_{\alpha=r, \cos \beta=s} &= 0 \\ \frac{\partial}{\partial \cos \beta} \omega(\alpha, \cos \beta) \Big|_{\alpha=r, \cos \beta=s} &= 0 \end{aligned} \right\} (47)$$

The nature of the critical point  $(r, s)$  is related to the sign of the Wronskian determinant  $D_W$ :

$$D_W = \left[ \left( \frac{\partial^2 \omega}{\partial \alpha \partial \cos \beta} \right)^2 - \left( \frac{\partial^2 \omega}{\partial \alpha^2} \right) \left( \frac{\partial^2 \omega}{\partial^2 \cos \beta} \right) \right]_{\alpha=r, \cos \beta=s} \quad (48)$$

If  $D_W$  is positive then the critical point  $(r, s)$  represents a divergence; if  $D_W$  is negative then the critical point represents a shoulder. Unfortunately, this method does not allow us to determine the lineshape. Therefore, numerical calculations are required.

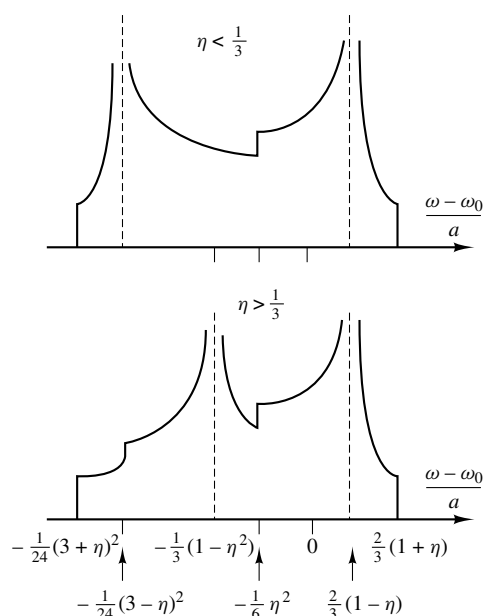


**Figure 6** Critical points determined by Stauss.<sup>32</sup> They are associated with the powder pattern of the central line in a static experiment;

$$a = -\frac{1}{6\omega_0} \left[ \frac{3\chi}{2I(2I-1)} \right]^2 \left[ I(I+1) - \frac{3}{4} \right]$$

### 6.1 Powder Pattern for a Pair of Satellite Lines

For static samples,<sup>27</sup> numerical calculations are based on the summation of signals for the direction of each crystallite. The two Euler angles are redefined by  $\alpha = 2\pi p/300$  and  $\cos \beta = p/300$ , where  $p = 0, \dots, 300$ . For each value of  $\eta$ , the summation is performed on

$$\omega_{m-1,m}^{(1)\text{static}} \left/ \frac{3\chi(1-2m)}{8I(2I-1)} \right. = 3 \cos^2 \beta - 1 + \eta \sin^2 \beta \cos 2\alpha \quad (49)$$

A satellite lineshape is shown in Figure 4. The positions of the shoulder and divergence<sup>13</sup> are derived from equations (47) and (48). The powder pattern of a pair of satellite lines for several values of  $\eta$  is plotted in Figure 5.

### 6.2 Powder Pattern for the Central Line

The critical points in the powder pattern of the central line have been determined for the two experiments. For a static sample, they have been determined by Stauss.<sup>32</sup> Two patterns (Figure 6) appear according to the value of  $\eta$  compared with  $\frac{1}{3}$ ; for example, for <sup>39</sup>K in inorganic potassium salts<sup>33</sup> or <sup>139</sup>La in lanthanum salts.<sup>34</sup> It is worth noting that these critical points depend neither on the convention for  $\eta$  nor on the choice of Euler angles: changing  $\eta$  to  $-\eta$  yields the same set of critical points. For a rotating sample, these points have been determined by Müller.<sup>31</sup> As previously, two powder patterns (Figure 7) appear, depending on the value of  $\eta$  compared with  $\frac{3}{7}$ . These patterns are clearly observed in <sup>27</sup>Al compounds.<sup>35</sup>

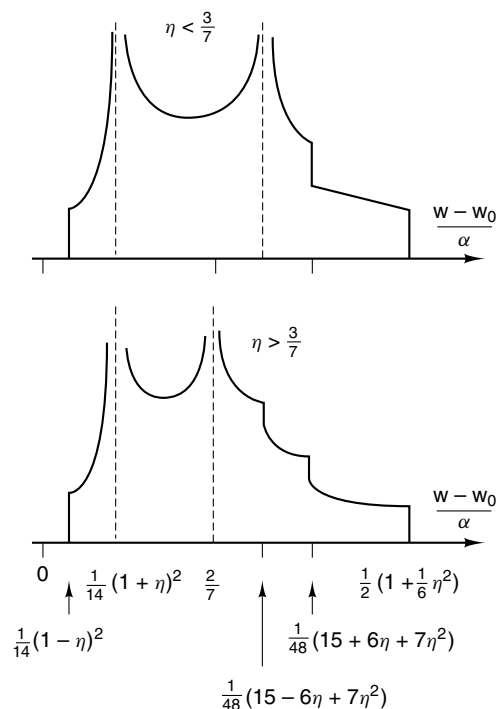


**Figure 7** Corrected critical points<sup>9,11</sup> determined by Müller.<sup>31</sup> They are associated with the powder pattern of the central line in a MAS experiment;

$$a = -\frac{1}{6\omega_0} \left[ \frac{3\chi}{2I(2I-1)} \right]^2 \left[ I(I+1) - \frac{3}{4} \right]$$

The powder pattern of the central line is obtained as in the previous case using equation (33) for a static sample or equation (43) for a rapidly rotating sample. To facilitate the comparison, the two sets of spectra are superposed as shown in Figure 8. We can see that the linewidth is reduced by a factor ranging from 2 to 4, depending on the value of  $\eta$  when a MAS experiment is performed (see *Line Narrowing Methods in Solids*). From a practical point of view, the asymmetry parameter of an experimental spectrum can be estimated by comparing the lineshape with those in Figure 8. Then the quadrupolar coupling constant can be calculated using the positions of the experimental critical points and those represented in Figures 6 and 7. Other simple procedures are also defined for extracting quadrupolar parameters from the spectra of static<sup>36</sup> or rotating<sup>37</sup> samples.

The second-order quadrupolar shift of the center of gravity  $\omega_{\text{iso}}(m-1, m)$  of the powder pattern is determined as follows:<sup>1</sup>

$$\begin{aligned} \omega_{\text{iso}}(m-1, m) &= \frac{1}{4\pi} \int_0^\pi d\beta \sin \beta \int_0^{2\pi} d\alpha \omega_{m-1,m}^{(2)\text{MAS}} \\ &= -\frac{3}{40\omega_0} \left[ \frac{\chi}{I(2I-1)} \right]^2 \left( 1 + \frac{1}{3}\eta^2 \right) \\ &\quad \times [I(I+1) - 9m(m-1) - 3] \quad (50) \end{aligned}$$

From a practical point of view, the experimental chemical shift of the center of gravity associated with the transition  $(m-1, m)$ ,  $\delta_{\text{CG}}^{\text{exp}}(m-1, m)$ , consists of two terms: the true chemical shift  $\delta_{\text{CS}}(m-1, m)$  and the contribution from the second-order

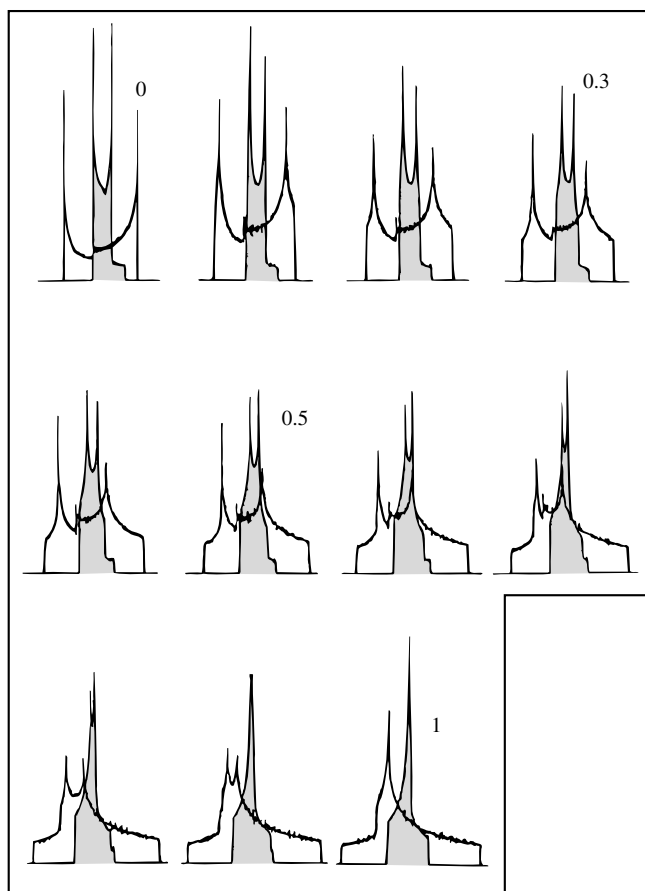


**Figure 8** Superposition of simulated powder patterns of the central line during static and MAS (shaded spectra) experiments for increasing values of the asymmetry parameter  $\eta$  from 0 to 1 in steps of 0.1

quadrupolar shift  $\omega_{\text{iso}}(m-1, m)/\omega_0$ . Thus,

$$\delta_{\text{CS}}(m-1, m) = \delta_{\text{CG}}^{\text{exp}}(m-1, m) - \omega_{\text{iso}}(m-1, m)/\omega_0 \quad (51)$$

For the central line, equation (51) becomes equation (1).

## 7 APPENDIX

The Euler angles are extensively used in the study of the quadrupolar interaction, especially in MAS, VAS, DAS, and DOR. They are defined as three successive positive angles of rotation for the coordinate frame (c.f.) as described in Figure 9. First [(Figure 9a)], the starting c.f. ( $x, y, z$ ), called the old c.f., in which we know the components  $V_k^{\text{OLD}}$  of the spherical tensor  $\mathbf{V}$ , is rotated counterclockwise around the  $z$  axis by an angle  $\alpha$ . This rotation generates a new c.f. ( $X, Y, z$ ). Then [(Figure 9b)] the counterclockwise rotation of this intermediate c.f. around the  $Y$  axis by an angle  $\beta$  generates a second intermediate c.f. ( $X', Y, z'$ ). Finally [(Figure 9c)], this second intermediate c.f. is rotated counterclockwise by an angle  $\gamma$  around the  $z'$  axis, resulting in a c.f. ( $x', y', z'$ ), called the new c.f., in which we wish to know the components  $V_j^{\text{NEW}}$  of the spherical tensor  $\mathbf{V}$ . It is worth noting that, in this definition of the Euler angles,  $\beta$  and  $\alpha$  also represent the polar angles of the  $z'$  axis in the old coordinate frame.

**Table 2** Wigner rotation matrix  $\mathcal{D}_{p,q}^{(2)}$  ( $\alpha, \beta, \gamma$ ), identical to that used by Spiess,<sup>20</sup> Mehring,<sup>21</sup> and Doane,<sup>38</sup> but the transposed and complex conjugate of that used by Haeberlen,<sup>19</sup> equal to  $\mathcal{D}_{p,q}^{(2)}$  ( $-\alpha, -\beta, -\gamma$ ) used by Freude and Haase<sup>9</sup>

$p$	$q$	1	0	-1	-2
2	2	$\frac{1}{4}(1 + \cos \beta)^2 e^{-2i(\alpha + \gamma)}$	$\sqrt{\frac{3}{8}} \sin^2 \beta e^{-2i\alpha}$	$-\frac{1}{2}(1 - \cos \beta) \sin \beta e^{-i(2\alpha + \gamma)}$	$\frac{1}{4}(1 - \cos \beta)^2 e^{-2i(\alpha - \gamma)}$
1	1	$\frac{1}{2}(1 + \cos \beta) \sin \beta e^{-i(\alpha + 2\gamma)}$	$-\sqrt{\frac{3}{8}} \sin 2\beta e^{-i\alpha}$	$[\frac{1}{2}(1 + \cos \beta) - \cos^2 \beta] e^{-i(\alpha + \gamma)}$	$-\frac{1}{2}(1 - \cos \beta) \sin \beta e^{-i(\alpha - 2\gamma)}$
0	0	$\sqrt{\frac{3}{8}} \sin^2 \beta e^{-2i\gamma}$	$\frac{1}{2}(3 \cos^2 \beta - 1)$	$-\sqrt{\frac{3}{8}} \sin 2\beta e^{i\gamma}$	$\sqrt{\frac{3}{8}} \sin^2 \beta e^{2i\gamma}$
-1	-1	$\frac{1}{2}(1 - \cos \beta) \sin \beta e^{i(\alpha - 2\gamma)}$	$\sqrt{\frac{3}{8}} \sin 2\beta e^{i\alpha}$	$[\frac{1}{2}(1 + \cos \beta) - \cos^2 \beta] e^{i(\alpha + \gamma)}$	$-\frac{1}{2}(1 + \cos \beta) \sin \beta e^{i(\alpha + 2\gamma)}$
-2	-2	$\frac{1}{4}(1 - \cos \beta)^2 e^{2i(\alpha - \gamma)}$	$\sqrt{\frac{3}{8}} \sin^2 \beta e^{2i\alpha}$	$\frac{1}{2}(1 - \cos \beta) \sin \beta e^{i(2\alpha + \gamma)}$	$\frac{1}{4}(1 + \cos \beta)^2 e^{2i(\alpha + \gamma)}$

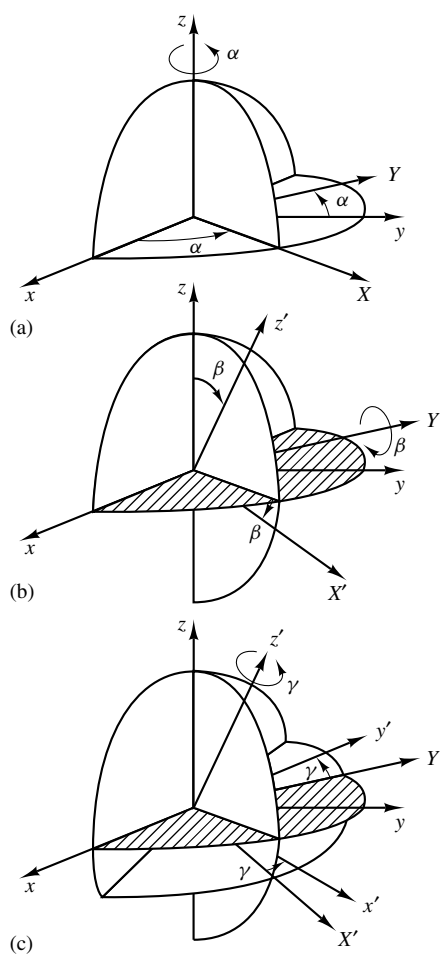


**Figure 9** Euler angles defining positive rotation of the coordinate frame  $(x, y, z)$ . They are used by Narita and co-workers,<sup>27</sup> Spiess,<sup>20</sup> Doane,<sup>38</sup> and Freude and Haase.<sup>9</sup> The angles  $\beta$  and  $\alpha$  are the polar angles of the  $z'$  axis in  $(x, y, z)$

As explained by Spiess,<sup>20</sup> the mathematical tool for expressing the components of the same spherical tensor  $\mathbf{V}$  in two different coordinate frames, where the new c.f. is obtained by three positive angles of rotation ( $\alpha, \beta, \gamma$ ) of the old one, is the Wigner rotation matrix  $\mathcal{D}_{p,q}^{(2)}(\alpha, \beta, \gamma)$  reported in Table 2. This matrix relates the components  $V_j^{\text{NEW}}$  of the spherical tensor in the new c.f. to the known components  $V_k^{\text{OLD}}$  of the same tensor in the old one by the relationships<sup>20,21,38,39</sup>

$$V_j^{\text{NEW}} = \sum_{k=-2}^2 \mathcal{D}_{k,j}^{(2)}(\alpha, \beta, \gamma) V_k^{\text{OLD}} \quad (52)$$

with the summation over the first subscript.

Figure 10 shows the Euler angles used by Baugher and co-workers.<sup>13,15</sup> First [(Figure 10a)], as in the previous definition, the old c.f.  $(x, y, z)$  is rotated counterclockwise by an angle  $\phi$  around the  $z$  axis, generating an intermediate c.f.  $(X, Y, z)$ . Then [(Figure 10b)] this intermediate c.f. is rotated counterclockwise, this time around the  $X$  axis, by an angle  $\theta$ , generating a second intermediate c.f.  $(X, Y', z')$ . Finally [(Figure 10c)], a counterclockwise rotation of this second intermediate c.f. around the  $z'$  axis by an angle  $\psi$  produces the new c.f.  $(x', y', z')$ . In contrast to the previous definition,

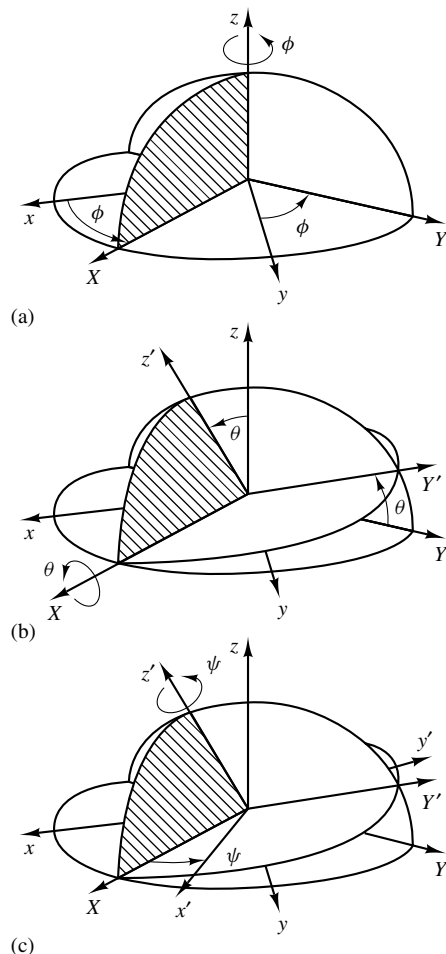


**Figure 10** Euler angles used by Baugher and co-workers<sup>13,15</sup> and Stauss,<sup>32</sup> and defined by Goldstein.<sup>14</sup> The angles  $\theta$  and  $\phi$  are not the polar angles of the  $z'$  axis in  $(x, y, z)$

$\theta$  and  $\phi$  are not the polar angles of the  $z'$  axis in the old coordinate frame. In Figure 9,  $\alpha$  is the angle relating the  $y$  axis and the line of nodes  $Y$ , whereas in Figure 10,  $\phi$  is the angle relating the  $x$  axis and the line of nodes  $X$ . These two angles are related by  $\alpha + \frac{1}{2}\pi = \phi$ . In other words,  $\alpha + \frac{1}{2}\pi$  and  $\phi$  correspond to the angle connecting the  $x$  axis with the line of nodes. As a result,  $\cos 2\phi = -\cos 2\alpha$ . This explains the change of sign for the terms containing  $\eta$  in equations (30) and (34), as in the paper of Baugher and co-workers.<sup>15</sup>

## 8 RELATED ARTICLES

Biological Systems: Spin-3/2 Nuclei; Boron NMR; Dynamic Frequency Shift; Germanium, Tin, and Lead NMR; Lithium NMR; Overtone Spectroscopy of Quadrupolar Nuclei; Oxygen-17 NMR; Oxygen-17 NMR: Applications in Biochemistry; Quadrupolar Nuclei in Solids; Quadrupolar Transition Metal and Lanthanide Nuclei; Shielding Calculations: Perturbation Methods; Sodium-23 NMR; Sulfur, Selenium, and Tellurium NMR; Magic Angle Spinning Carbon-13 Lineshapes: Effect of Nitrogen-14; Magic Angle Spinning: Effects of Quadrupolar Nuclei

on Spin-1/2 Spectra; Relaxation Theory for Quadrupolar Nuclei; Tritium NMR; Quadrupolar Coupling: An Introduction and Crystallographic Aspects; Quadrupolar Metal Nuclides in Bioinorganic Chemistry: Solid-State NMR Studies; Oxygen-17 NMR Studies of Organic and Biological Molecules; Laszlo, Pierre: Getting Acquainted with a Spin-3/2 Nucleus.

## 9 REFERENCES

1. A. Samoson, *Chem. Phys. Lett.*, 1985, **119**, 29.
2. E. Lippmaa, A. Samoson, and M. Mägi, *J. Am. Chem. Soc.*, 1986, **108**, 1730.
3. F. Lefebvre, J. P. Amoureux, C. Fernandez, and E. G. Derouane, *J. Chem. Phys.*, 1987, **86**, 6070.
4. D. Massiot, A. Kahn-Harari, D. Michel, D. Müller, and F. Taulelle, *Magn. Reson. Chem.*, 1990, **28**, S82.
5. B. Q. Sun, J. H. Baltisberger, Y. Wu, A. Samoson, and A. Pines, *Solid State Nucl. Magn. Reson.*, 1992, **1**, 267.
6. P. P. Man, *Chem. Phys. Lett.*, 1990, **168**, 227.
7. B. C. Sanctuary and T. K. Halstead, in 'Advances in Magnetic and Optical Resonance', ed. W. S. Warren, Academic Press, San Diego, 1990, Vol. 15, p. 79.
8. A. P. M. Kentgens, *J. Magn. Reson. A*, 1993, **104**, 302.
9. D. Freude and J. Haase, in 'NMR Basic Principles and Progress', eds P. Diehl, E. Fluck, H. Günter, R. Kosfeld, and J. Seelig, Springer-Verlag, Berlin, 1993, Vol. 29.
10. J. L. Dye, A. S. Ellaboudy, and J. Kim, in 'Modern NMR Techniques and their Application in Chemistry', eds A. I. Popov and K. Hallenge, Marcel Dekker, New York, 1991.
11. G. Engelhardt and D. Michel, 'High-Resolution Solid-State NMR of Silicates and Zeolites', Wiley, Chichester, 1987.
12. G. E. Jellison, Jr., S. A. Feller, and P. J. Bray, *J. Magn. Reson.*, 1977, **27**, 121.
13. P. C. Taylor, J. F. Baugher, and H. M. Kriz, *Chem. Rev.*, 1975, **75**, 203.
14. H. Goldstein, 'Classical Mechanics', 2nd edn., Addison-Wesley, Reading, MA, 1980.
15. J. F. Baugher, P. C. Taylor, T. Oja, and P. J. Bray, *J. Chem. Phys.*, 1969, **50**, 4914.
16. C. P. Slichter, 'Principles of Magnetic Resonance', 3rd edn., Springer-Verlag, New York, 1990.
17. M. H. Cohen and F. Reif, in 'Solid State Physics', eds F. Seitz and D. Turnbull, Academic Press, New York, 1957, Vol. 5.
18. A. Abragam, 'The Principles of Nuclear Magnetism', Oxford University Press, Oxford, 1961.
19. U. Haeberlen, 'High Resolution NMR in Solids. Selective Averaging', Academic Press, New York, 1976.
20. H. W. Spiess, in 'NMR Basic Principles and Progress', eds P. Diehl, E. Fluck, and R. Kosfeld, Springer-Verlag, Berlin, 1978, Vol. 15.
21. M. Mehring, 'Principles of High Resolution NMR in Solids', 2nd edn., Springer-Verlag, Berlin, 1983.
22. A. Samoson and E. Lippmaa, *Phys. Rev. B*, 1983, **28**, 6567.
23. A. Samoson, E. Kundla, and E. Lippmaa, *J. Magn. Reson.*, 1982, **49**, 350.
24. H. J. Behrens and B. Schnabel, *Physica B*, 1982, **114**, 185.
25. P. P. Man, H. Théveneau, and P. Papon, *J. Magn. Reson.*, 1985, **64**, 271.
26. B. A. Huggins and P. D. Ellis, *J. Am. Chem. Soc.*, 1992, **114**, 2098.
27. K. Narita, J. Umeda, and H. Kusumoto, *J. Chem. Phys.*, 1966, **44**, 2719.
28. J. Hirschinger, P. Granger, and J. Rosé, *J. Phys. Chem.*, 1992, **96**, 4815.
29. P. J. Chu and B. C. Gerstein, *J. Chem. Phys.*, 1989, **91**, 2081.
30. F. Wolf, D. Kline, and H. S. Story, *J. Chem. Phys.*, 1970, **53**, 3538.
31. D. Müller, *Ann. Phys. (Leipzig)*, 1982, **39**, 451.
32. G. H. Stauss, *J. Chem. Phys.*, 1964, **40**, 1988.
33. T. J. Bastow, *J. Chem. Soc., Faraday Trans.*, 1991, **87**, 2453.
34. B. Herreros, P. P. Man, J. M. Manoli, and J. Fraissard, *J. Chem. Soc., Chem. Commun.*, 1992, 464.
35. J. Skibsted, E. Henderson, and H. J. Jakobsen, *Inorg. Chem.*, 1993, **32**, 1013.
36. P. Granger, *Magn. Reson. Chem.*, 1990, **28**, 156.
37. G. Engelhardt and H. Koller, *Magn. Reson. Chem.*, 1991, **29**, 941.
38. J. W. Doane, in 'Magnetic Resonance of Phase Transitions', eds F. J. Owens, C. P. Poole, Jr., and H. A. Farach, Academic Press, New York, 1979.
39. D. M. Brink and G. R. Satchler, 'Angular Momentum', 2nd edn., Clarendon Press, Oxford, 1968, p. 51.

### Biographical Sketch

Pascal P. Man. b 1952. Ph.D., 1982, Materials Science, Sc.D., 1986, physics, Université Pierre et Marie Curie, Paris, France. Introduced to NMR by H. Zanni. Postdoctoral work at University of Cambridge (with J. Klinowski). Université Pierre et Marie Curie, 1988–present. Approx. 80 publications. Current research speciality: solid state NMR on quadrupolar nuclei and its applications in heterogeneous catalysts.